

Article

# TiO<sub>2</sub>@PEI-Grafted-MWCNTs Hybrids Nanocomposites Catalysts for CO<sub>2</sub> Photoreduction

Caterina Fusco <sup>1,\*</sup> , Michele Casiello <sup>2</sup> , Lucia Catucci <sup>2</sup> , Roberto Comparelli <sup>3</sup> ,  
Pietro Cotugno <sup>2</sup> , Aurelia Falcicchio <sup>4</sup>, Francesco Fracassi <sup>2</sup>, Valerio Margiotta <sup>3</sup>,  
Anna Moliterni <sup>4</sup>, Francesca Petronella <sup>3</sup> , Lucia D'Accolti <sup>1,2,\*</sup>  and Angelo Nacci <sup>1,2,\*</sup> 

<sup>1</sup> ICCOM-CNR (Istituto di Chimica dei Composti OrganoMetallici-Consiglio Nazionale delle Ricerche), SS Bari, Via Orabona 4, 70126 Bari, Italy

<sup>2</sup> Dipartimento di Chimica, Università di Bari "A. Moro", Via Orabona 4, 70126 Bari, Italy; michele.casiello@uniba.it (M.C.); lucia.catucci@uniba.it (L.C.); pietro.cotugno@uniba.it (P.C.); francesco.fracassi@uniba.it (F.F.)

<sup>3</sup> IPCF-CNR (Istituto per i Processi Chimico Fisici-Consiglio Nazionale delle Ricerche), SS Bari, Via Orabona 4, 70126 Bari, Italy; r.comparelli@ba.ipcf.cnr.it (R.C.); v.margiotta@ba.ipcf.cnr.it (V.M.); f.petronella@ba.ipcf.cnr.it (F.P.)

<sup>4</sup> CNR-IC (Consiglio Nazionale delle Ricerche-Istituto di Cristallografia), Via Amendola 122/O, 70126 Bari, Italy; a.falcicchio@ic.cnr.it (A.F.); a.moliterni@ic.cnr.it (A.M.)

\* Correspondence: fusco@ba.iccom.cnr.it (C.F.); lucia.daccolti@uniba.it (L.D.); angelo.nacci@uniba.it (A.N.); Tel.: +39-080-544-2068 (C.F.); +39-080-544-2068 (L.D.); +39-080-544-2499 (A.N.)

Received: 19 January 2018; Accepted: 13 February 2018; Published: 20 February 2018

**Abstract:** Anatase (TiO<sub>2</sub>) and multiwalled carbon nanotubes bearing polyethylenimine (PEI) anchored on their surface were hybridized in different proportions according to a sol-gel method. The resulting nanocomposites (TiO<sub>2</sub>@PEI-MWCNTs), characterized by BET, XRD, XPS, SEM, and UV techniques, were found efficient catalysts for CO<sub>2</sub> photoreduction into formic and acetic acids in water suspension and under visible light irradiation. PEI-grafted nanotubes co-catalysts are believed to act as CO<sub>2</sub> activators by forming a carbamate intermediate allowing to accomplish the first example in the literature of polyamines/nanotubes/TiO<sub>2</sub> mediated CO<sub>2</sub> photoreduction to carboxylic acids.

**Keywords:** artificial photosynthesis; capture and valorization of CO<sub>2</sub>; MWCNTs hybrids nanocomposites

## 1. Introduction

During the past decade, great deal of attention has been dedicated to converting solar energy into chemical energy in the form of so-called "solar fuels", such as H<sub>2</sub>, methanol, methane, formic acid, etc. In this context, the reduction of carbon dioxide is gaining more and more importance in the research area of chemistry and materials, not only for solving the problems resulting from environmental pollution, but also for finding ways to maintain the carbon resources which are being depleted by the burning of fossil fuels [1].

A very promising method is the photoreduction of CO<sub>2</sub> to produce clean hydrocarbon fuels under sunlight irradiation, a process that mimics the natural photosynthesis in plants. Among all photocatalysts, anatase TiO<sub>2</sub> still remains the most promising candidate considering its photostability, corrosion resistance, low cost, and strong oxidation power [2–4].

However, photocatalytic efficiency of TiO<sub>2</sub> is limited due to its large band gap (3.2 eV), which can only be excited under ultraviolet irradiation and rapid recombination of photoinduced electrons and holes. To solve these problems, a variety of dopants has been investigated, ranging from transition metals (e.g., Pd, Pt, Fe, etc.) [5–10] and their oxides (e.g., Cu<sub>2</sub>O, CeO<sub>2</sub>, etc.), [11] to non-metal ions (N and I) [12] and rare earth derivatives (La<sub>2</sub>O<sub>3</sub>) [13].

During the past decade, there has been a growing interest in hybridizing TiO<sub>2</sub> with carbon nanostructured materials, such as nanotubes (CNTs) [14–18] and graphene [19], that play the role of transferring photogenerated electrons from the TiO<sub>2</sub>, suppressing the recombination rate of the electron–hole pairs. Recently, a new strategy is emerging concerning the modification of TiO<sub>2</sub> with co-catalysts capable of enhancing CO<sub>2</sub> adsorption [20]. Main approaches are based on metal oxides (mainly MgO) [21,22], metal organic framework (MOFs) [23] and amines [24,25].

In this context, being carbon nanotubes amongst the most promising solid sorbents for CO<sub>2</sub> capture [26,27], in particular when their walls are decorated with CO<sub>2</sub>-philic groups [28–32], we sought to enhance photocatalytic performance of titania by means of its conjugation with carbon nanotubes bearing polyamines anchored on their surface, with the specific task of adsorbing the CO<sub>2</sub> reactant and help the redox process.

With this in mind, in our ongoing efforts aimed at searching new green catalytic methods [33–38], we prepared a series of hybridized materials based on anatase and amine-grafted multiwalled carbon nanotubes (TiO<sub>2</sub>@amine-MWCNTs) and tested their ability to serve as an efficient catalyst for photoreduction of carbon dioxide.

## 2. Materials and Methods

### 2.1. Chemicals

Common commercial solvents and reagents of high purity were employed. Commercial Caroat<sup>®</sup> (Pullach, Germany) triple salt (2KHSO<sub>5</sub>·KHSO<sub>4</sub>·K<sub>2</sub>SO<sub>4</sub>), a gift from Peroxid-Chemie (Degussa, Germany), was the source of potassium monoperoxysulfate (caroate) for the synthesis of TFDO [39,40]. MWCNTs (purity >90 wt.%, diameter between 0.7 and 1.4 nm) are commercially available from Sigma-Aldrich (Milan, Italy) in form of powder.

Carbon dioxide, O<sub>2</sub>, Argon and Helium were with purity of 99.99%, a gas burette (Figure S1) was used to measure gas volume in adsorption/desorption experiments. Formic and acetic acid analyses were performed with an Ion Chromatograph Dionex DX120 (Ion Pac ICE-AS6 Analytical Column, Monza, Italy); 0.8 mM heptafluorobutyric acid (Sigma-Aldrich) was used as eluent (flow 1.00 mL/min) and 5.0 mM tetrabutylammonium hydrate (Sigma-Aldrich) as regenerating eluent (flow 4.5 mL/min).

Formic acid 99% and acetic acid (Sigma Aldrich) were employed as standard for building IC calibration curves. Analyses were carried out by using a sample loop of 25 µL, with a column pressure less than 640 PSI and a background of 35–40 µS.

GC analyses for liquid and gas phase were performed with a GC Tracera Shimadzu 2010 (Milan, Italy) with a Detector BID-2010 (Shimadzu, Milan, Italy) plus and a Micropacked ST column (temperature program isotherm at 40 °C 30 min). Infrared analyses were performed in the range 400–4000 cm<sup>-1</sup> (64 scans), using a PerkinElmer 2000 FT-IR spectrometer (Milan, Italy).

### 2.2. Physico-Chemical and Morphological Characterization of Nanocomposites

Thermogravimetric analyses were recorded on a TGA Q500 (TA Instruments, New Castle, GA, USA) using a flowing nitrogen atmosphere. The samples (about 1 mg per sample) were equilibrated at 100 °C for 20 min and then heated at a rate of 10 °C min<sup>-1</sup> up to 800 °C.

Elemental analyses were performed on a Thermo Flash EA 1112 series CHNS-O elemental analyzer (Monza, Italy) with an accepted tolerance of 0.4 units.

TEM (Transmission electron microscopy) analyses were performed with a TEM Philips EM208 instrument (Vienna, Austria) using an accelerating voltage of 100 kV. The samples were prepared by dropping aliquots of the DMF dispersions onto TEM grids (200 mesh, Nichel, carbon only, Ted Pella, Milan, Italy).

BET (Brunauer-Emmett-Teller) specific surface area was obtained by N<sub>2</sub> adsorption-desorption method on powder samples using a Micromeritics TriStar II 3020 (Micromeritics, Norcross, U.S.A.). The samples (500 mg) were pre-treated at 80 °C for 2 h before N<sub>2</sub> adsorption.

FE-SEM investigations were performed by a Zeiss Sigma (Milan, Italy) microscope operating in the range 0.5–20 kV and equipped with an in-lens secondary electron detector. FE-SEM samples were prepared by sticking the powder on double sided carbon tape. Samples were mounted onto stainless-steel sample holders by using and grounded by silver paste.

UV-Vis diffuse reflectance spectra were recorded with a UV-vis-NIR Cary 5 (Varian, Palo Alto, CA, USA) spectrophotometer equipped with an integrating sphere (BaSO<sub>4</sub>).

X-Ray powder diffraction data were collected at room temperature by using an automated Rigaku RINT2500 laboratory diffractometer (50 KV, 200 mA, Neu-Isenburg, Germany) equipped with the silicon strip Rigaku D/teX Ultra detector. Detailed XRD analyses of hybrids nanocomposites are showed in Figure S2.

X-ray photoelectron spectroscopy (XPS) analyses were performed on a PHI VersaProbe II spectrometer (Physical Electronics, Kanagawa, Japan) equipped with a monochromatic Al K $\alpha$  X-ray source (1486.6 eV) operating at a spot size of 100  $\mu$ m, corresponding to a power of 24.4 W. Survey (0–1400 eV) and high resolution (C 1s, O 1s, N 1s, Ti 2p, Cl 2p, F 1s) spectra were recorded in FAT (fixed analyzer transmission) mode at pass energy of 117.4 eV and 46.95 eV, respectively. All spectra were acquired at a take-off angle of 45° with respect to the sample normal. Dual-beam charge neutralization was constantly applied during analysis. Charge correction of the spectra was performed by taking the sp<sup>2</sup> graphitic component of the C 1s spectrum as internal reference (binding energy, BE = 284.6 eV).

XPS analysis was repeated on three different spots for each sample. During analyses, special care was devoted to verifying that no change in the samples was induced by exposure to the X-ray beam and the charge neutralization dual-beam. Detailed spectra processing was performed by commercial MultiPak software (Version 9.5.0.8, 30-10-2013, Ulvac-PHI, Inc., Kanagawa, Japan). The high-resolution spectra were fitted with mixed Gaussian-Lorentzian peaks after a Shirley background subtraction.

The DO 9721 quantum photo-radiometer (Delta Ohm, Pordenone, Italy) and thermometer data logger were used for measuring illuminance, irradiance, luminance and temperature.

### 2.3. Preparation of ox-MWCNTs (2) with TFDO

Preparation was accomplished according to our previous method [41,42]. MWCNTs (600–1000 mg) were placed in CH<sub>2</sub>Cl<sub>2</sub> (50–100 mL) and the mixture was sonicated for 30 min. An aliquot (35 mmol) of the standardized cold solution of methyl(trifluoromethyl)dioxirane (TFDO, 70 mL, 0.5 M) in 1,1,1-trifluoropropanone (TFP), was then added in one portion to the mixture, which was stirred and kept at 0 °C. After 24 h the reaction was complete, the mixture was filtered, and ox-CNTs 2 were washed several times with CH<sub>2</sub>Cl<sub>2</sub> followed by MeOH, with recovery of 700–1300 mg.

### 2.4. Epoxide Ring Opening of ox-MWCNTs (2): Preparation of Amine-Grafted-MWCNTs 3 and 4

This procedure was used for preparation of amine grafted-MWCNTs 3 and 4 [41,42]. Oxidized nanotubes 2 (1 g) were dispersed in 1,6-hexamethylenediamine (3.7 g) or branched polyethylenimine (5 g PEI MW 600, 99% of purity) and the mixture was heated at reflux at 140 °C under N<sub>2</sub> for 12 h. Next, the reaction mixture was diluted with methanol (20 mL) and filtered through a PTFE membrane filter paper (0.2  $\mu$ m). The solid was washed several times with CH<sub>2</sub>Cl<sub>2</sub> followed by MeOH to remove any excess of amine leading to HMDA-MWCNTs (3, 1.20 g) or PEI-MWCNTs (4, 1.25 g). Elemental analyses for 3: C (95.45%), H (3.24%), O (0.30%), N (1.01%); for 4: C (91.59%), H (5.61%), O (0.17%), N (2.63%).

### 2.5. Preparation of hybrids nanocomposites photocatalysts 1A, 1C, 4A-C

Preparation of hybrids nanocomposites was accomplished to previous method [14], titanium tetrachloride (98% TiCl<sub>4</sub>), hydrochloric acid (38% HCl) and distilled water with a molar ratio of TiCl<sub>4</sub>:HCl:H<sub>2</sub>O = 0.1:1:200 were homogenized under magnetic stirring for 30 min. The thus obtained transparent mother solution was then used as the raw material for preparing nanocomposites for

photocatalytic experiments. Proper amounts of both p-MWCNTs (1) and functionalized PEI-MWCNTs (4) were separately dispersed into the proper volume of mother solution according to Table 1.

**Table 1.** Preparation of nanocomposites 1A, 1C and 4A-C.

Nanocomposite	MWCNTs	Amount of MWCNTs (mg)	TiCl <sub>4</sub> /HCl Mother Solution (mL)	Weight of Nanocomposite (g)	% (w/w) of PEI-MWCNTs in the Hybrid <sup>a</sup>
TiO <sub>2</sub> (blank)	–	–	250	–	–
TiO <sub>2</sub> @MWCNTs (1A)	p-MWCNTs (1)	20	250	1.0056	2.0%
TiO <sub>2</sub> @MWCNTs (1C)	p-MWCNTs (1)	500	500	1.6651	30%
TiO <sub>2</sub> @PEI-MWCNTs (4A)	PEI-MWCNTs (4)	20	250	1.1152	1.8%
TiO <sub>2</sub> @PEI-MWCNTs (4B)	PEI-MWCNTs (4)	200	500	1.9508	10.3%
TiO <sub>2</sub> @PEI-MWCNTs (4C)	PEI-MWCNTs (4)	500	500	1.6197	30.9%

<sup>a</sup> Evaluated based on the weights of suspended MWCNTs and recovered nanocomposites.

After suspension, mixture was sonicated and then ammonia was slowly added (until neutrality) under vigorous stirring, thus inducing TiO<sub>2</sub> precipitation and formation of random agglomerates by inclusion of CNTs [14]. After filtration, nanocomposites 1A, 1C and 4A-C were washed with distilled water and dried at 80 °C for 24 h.

### 2.6. Photocatalytic Experiments

The photocatalytic activities of samples 1A-C, 4A-C were evaluated by the reduction of CO<sub>2</sub> in H<sub>2</sub>O [9,43] (see Section 3.3). The apparatus used for the photocatalytic experiments consists of a three necked Pyrex batch photoreactor of cylindrical shape containing 20 mL of aqueous suspension. The photoreactor was provided with a jacket for cooling water circulation and ports in its upper section for the inlet and outlet of gases, for sampling and for pH and temperature measurements. A HRC UV-VIS lamp 300 W (Sanolux, Milan, Italy) and Xe-Halogen lamp 400 W (Radium, Milan, Italy) were placed in proximity (5–6 cm) of the reactor. Argon was bubbled for 30 min, to avoid the presence of air, and then CO<sub>2</sub> for approximately 60 min before switching on the lamps. The amounts of catalyst used were 150 and 500 mg in 20 mL of solution (loading of 7.5 and 25 mg/mL). The initial pH was 4.58. The temperature inside the reactor was held at approximately 25 °C by a continuous circulation of water in the jacket around the photoreactor. The photoreactivity runs lasted in 5.0 h and the products were detected by Ion Chromatography and GC-BID.

### 2.7. UBA Reduction Experiments

Experiments were performed following a protocol previously reported in literature [18,44,45]. The proper amount of the TiO<sub>2</sub>/MWCNTs powder was dispersed in a mixture of chloroform (61%) hexane (27%) and ethanol (12%), obtaining a concentration of 5000 ppm. Finally, the required volume of a stock solution of UBA in EtOH ( $2.5 \times 10^{-3}$  M) was added to reach the desired CHCl<sub>3</sub>:Hexane:EtOH ratio, and fix the final UBA concentration at  $10^{-5}$  M. Such a reaction mixture was poured in a quartz cuvette, sealed by a Teflon-faced rubber cap and purged under N<sub>2</sub> flow for 20 min, under stirring. Such a procedure has a twofold role: (i) to remove oxygen from the reaction environment and (ii) to promote the absorption-desorption equilibria between the photocatalyst and the UBA. Next, the mixture, was irradiated under continuous stirring with UV light using a medium pressure 200 W mercury lamp ( $\lambda > 250$  nm), equipped with neutral density filters in order to achieve a light flux of 5 mW/cm<sup>2</sup>. At scheduled time intervals, the cuvette was removed from the light source and the reaction mixture was transferred in a centrifuge tube under inert atmosphere. The UBA/photocatalyst suspension was separated by centrifugation, and the liquid phase analyzed by absorption spectroscopy. The reaction was monitored by recording difference absorption spectra of the irradiated reaction mixtures. Any change in the absorption line-shape was then clearly identified for each sample, by considering as reference the respective unphotolyzed solution.



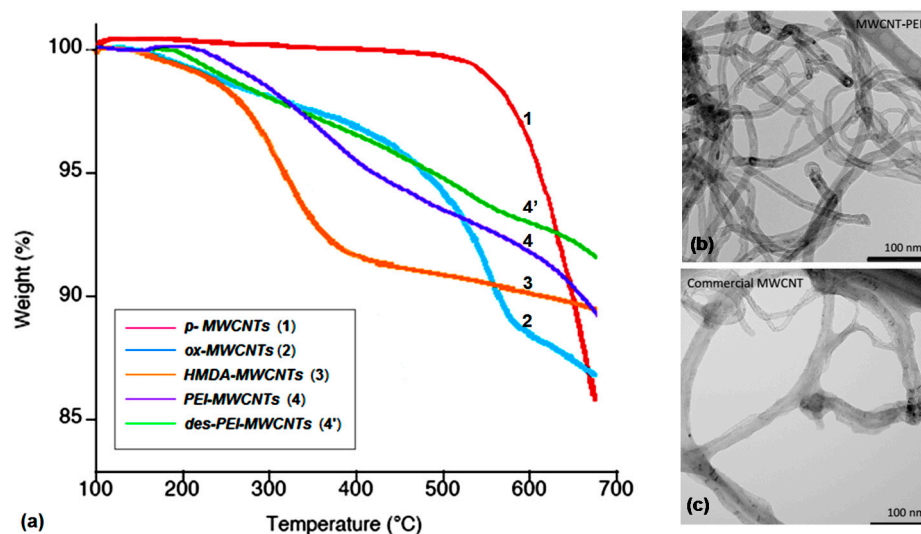


Figure 3. (a) TGA profiles of MWCNTs 1-4'; TEM images of (b) PEI-MWCNTs (4) and (c) p-MWCNTs (1).

The weight loss of 12.3% for desorbed PEI-MWCNTs (4') accounted for a substantial stability of grafted amines-CNTs under the CO<sub>2</sub> capture conditions. Moreover, comparison of TEM images of PEI-MWCNTs 4 (Figure 3b) and p-MWCNTs 1 (Figure 3c) revealed no substantial change in morphology upon surface functionalization of p-MWCNTs.

Loading of CO<sub>2</sub>-philic amine groups of modified MWCNTs 3-4 was evaluated by means of total N-content (%), whereas their sorbent capacity was estimated in a series of adsorption/desorption experiments and compared with that of pristine p-MWCNTs (1) (Table 2). As expected, grafting of amine moieties onto the surface of MWCNTs increased their sorbent capacity by conjugating physical adsorption of nanotubes and chemical absorption of CO<sub>2</sub>-philic functionalities. Additionally, results in Table 2 confirmed that the CO<sub>2</sub> capture process proved to be perfectly reversible for amine-grafted-MWCNTs 3-4, for which CO<sub>2</sub> could be quantitatively released at 80 °C.

Table 2. CO<sub>2</sub> adsorption/desorption ability of amine-grafted MWCNTs.

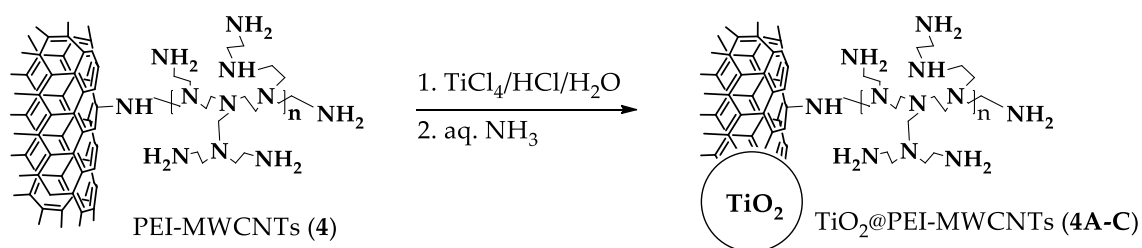
Amine-Grafted MWCNTs	N-Content (%) by elem. Analysis	Adsorbed CO <sub>2</sub> at 25 °C (mL·g <sup>-1</sup> ) <sup>a</sup>	Desorbed CO <sub>2</sub> at 80 °C (mL·g <sup>-1</sup> ) <sup>b</sup>
p-MWCNTs 1	–	11	11
HMDA-MWCNTs 3	1.01	24	24
PEI-MWCNTs 4	2.63	35	35

<sup>a</sup> Adsorption time 6 h. <sup>b</sup> Desorption time 3 h (see Supplementary Materials for details).

On these bases, also taking into account the recent literature [47] highlighting polyethylenimine as one of the greatest candidates for CO<sub>2</sub> sequestration processes, PEI-grafted MWCNTs 4 showing the best capture performance was selected as co-catalysts of titania in the CO<sub>2</sub> photoreduction.

### 3.2. Preparation and Characterization of Hybrid Nanocomposites Photocatalysts

Hybrid nanocomposites photocatalysts were prepared according to a sol-gel method [14]. At this end, functionalized nanotubes 4 were suspended in a aqueous HCl solution of TiCl<sub>4</sub> from which TiO<sub>2</sub> was precipitated by addition of ammonia, thus forming random agglomerates by inclusion of CNTs (Scheme 1) [13]. The ensuing TiO<sub>2</sub>@PEI-MWCNTs composites were collected by filtration, washed with distilled H<sub>2</sub>O and dried at 80 °C for 24 h. For the photocatalytic experiments, a number of hybrid nanocomposites were selected (1A, 1C, 4A-C) using different amounts of pristine nanotubes 1 and PEI-modified- MWCNTs 4, as listed in Table 3.



**Scheme 1.** Procedure for hybrid nanocomposites preparation.

**Table 3.** Hybrid nanocomposites preparation.

Hybrid <sup>a</sup>	% (w/w) of PEI-MWCNTs in the Hybrid	BET Surface Area (m <sup>2</sup> /g)
1A (control)	2.0% <sup>b</sup>	176.7
1C (control)	30% <sup>b</sup>	299.2
4A	1.8%	161.8
4B	10.3%	327.3
4C	30.9%	304.2

<sup>a</sup> See Table 1 for details. <sup>b</sup> Unmodified MWCNTs were hybridized as control composites.

Hybridized materials were characterized by BET, XRD, XPS, FE-SEM, and UV techniques (see Supplementary Materials for details). BET analyses displayed an expected trend in which the presence of carbon nanotubes remarkably increased the surface area of composites with respect to titania (Table 3).

XRD spectra were reported in Figure 4. The diffraction pattern of PEI-grafted MWCNTs **4** showed a very low degree of crystallinity (Figure 4a). The diffraction patterns of the two hybrid composites **1A** and **4A**, consisting of TiO<sub>2</sub> with minimal amounts (2%) of carbon nanotubes, exhibited similar features of anatase phase (Figure 4b). As expected, on increasing the PEI-MWCNTs content up to 10% (composite **4B**), the anatase polymorphic form did not persist anymore (Figure 4c), most likely because the increase of the almost amorphous nanotubes hinders the agglomeration of TiO<sub>2</sub> particles [14–18] (see Supplementary Materials for details).

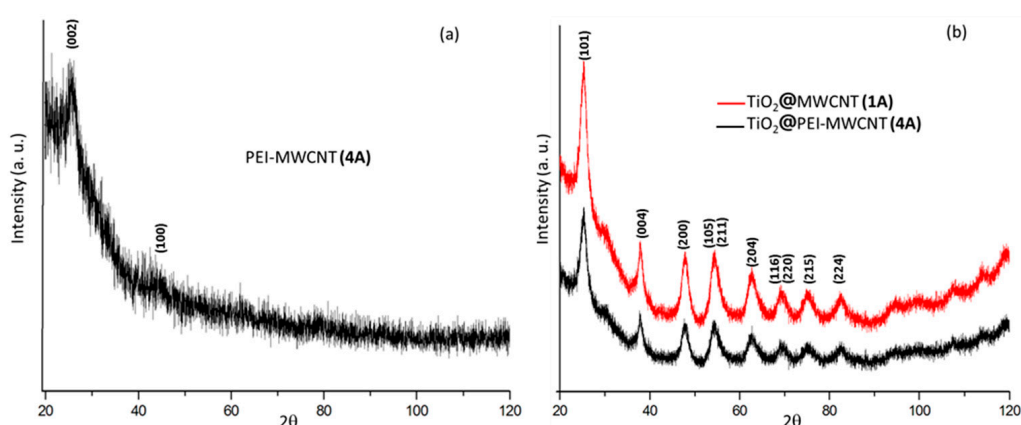


**Figure 4.** Cont.

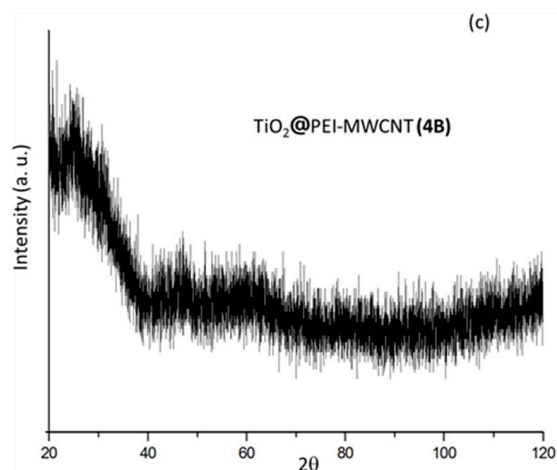


Figure 4. XRD patterns of samples (a) **4**; (b) **1A**; (c) **4A-B**.

XPS analyses showed the expected surface atomic concentration of composites (Table 4). Notably, from both atomic percentages and high-resolution N1s signals (Figure S3) emerged that PEI-MWCNTs-TiO<sub>2</sub> composite did not undergo to a sensible variations of its surface composition after catalytic reaction. The N1s signal could be curve fitted with two components: a dominant component at  $400.5 \pm 0.2$  eV ascribed to amino groups and a minor component centred at  $402.2 \pm 0.2$  eV that could be due to protonated amino groups or to amino groups involved in hydrogen bonding. This is a clear evidence of photocatalyst stability under the reaction conditions.

Table 4. XPS analyses of hybrid nanocomposites.

Sample	Surface Atomic Concentrations (%)			
	C	O	N	Ti
PEI-MWCNTs ( <b>4</b> )	$85.8 \pm 0.5$	$6.8 \pm 0.2$	$7.4 \pm 0.2$	–
TiO <sub>2</sub> @PEI-MWCNTs ( <b>4C</b> )	$55.2 \pm 0.6$	$30.6 \pm 0.6$	$3.7 \pm 0.3$	$10.5 \pm 0.3$
TiO <sub>2</sub> @PEI-MWCNTs ( <b>4C</b> ) *	$59.8 \pm 0.6$	$27.6 \pm 0.5$	$3.3 \pm 0.2$	$9.3 \pm 0.3$

\* After reaction.

SEM images of samples **1A** and **4C** (Figure S4) showed heterogeneous samples consisting of MWCNTs randomly dispersed into TiO<sub>2</sub> agglomerates. A high level of magnification (Figure S4(D)) highlights the close interfacial contact between nanotubes and TiO<sub>2</sub> which is crucial for narrowing of titania bandgap and consequently for the enhancement of catalytic activity [48].

UV-Vis reflectance spectra of TiO<sub>2</sub>, TiO<sub>2</sub>@MWCNTs (**1C**) and TiO<sub>2</sub>@PEI-MWCNTs (**4C**) recorded in absorption mode are presented in Figure 5. As expected, all hybrid materials showed a higher light absorption capability in the UV region below 400 nm, due to the characteristic absorption of TiO<sub>2</sub>. Remarkably, spectra of **1C** and **4C** appear to be quite similar, displaying the same red shift effect caused by the incorporation of both nanotubes alone and PEI-modified-CNTs into TiO<sub>2</sub> [49–51]. This means that the formation of covalent bonds between MWCNTs and PEI in **4C** does not introduce significant modifications of graphite-like structure of nanotubes. However, the composite **4C** showed a more intense absorption underneath 350 nm, maybe due to the auxochrome effect (mainly  $n \rightarrow \sigma^*$  electronic transitions) of amino and hydroxyl groups linked on nanotubes surface. This effect could explain the enhanced photoreducing power displayed by composite **4C** in the photoreduction of the organic dye UBA in the UV range (see mechanistic insights paragraph).

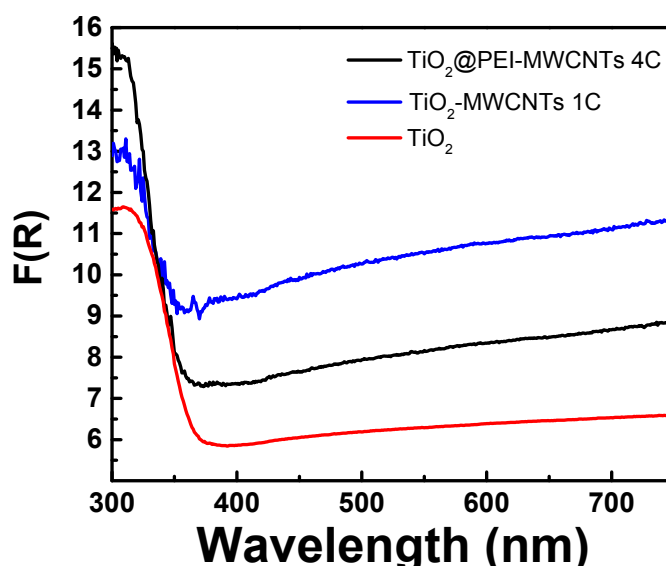


**Figure 5.** Absorbance spectra in Kubelka-Munk units of photocatalytic materials.

### 3.3. Photocatalytic Experiments

Photocatalytic conditions were chosen according to the goal of this study: the development of a metal free catalyst system that mimics the natural photosynthetic process, i.e., ambient temperature, sunlight radiation and water as the hydrogen source.

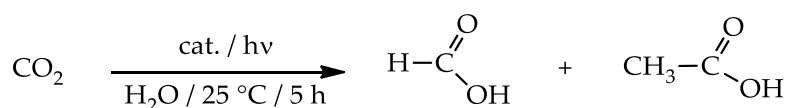
As a further aim of this work, we attempted to investigate the influence of radiation source on photocatalysis using two different emitting lamps: (i) the SANOLUX lamp, displaying a higher radiance in the near UV (315–400 nm) and the Xe-Halogen lamp, possessing the major emission power in the visible range (400–700 nm, see Figure S6 in Supplementary Materials).

Photoreduction was performed in a water phase suspension (20 mL) of the solid catalyst (with the loading in the range of 7.5–30 mg<sub>solid.cat.</sub>/mL), and monitoring reaction parameters and species produced in both the liquid solution and in the gas phase of the reactor head space [43] (see Figure S5).

Argon was initially bubbled for 30 min, to avoid the presence of air, then CO<sub>2</sub> for approximately 60 min, to saturate the reaction mixture, upon which suspension was irradiated for 5 h under vigorous stirring at room temperature. Initial pH value of solution after bubbling was found to be equal to 4.78, and raised to 5.80 after reaction.

Under the chosen conditions, nanocomposites proved to be active in converting CO<sub>2</sub> into formic and acetic acids (Scheme 2), while neither simple PEI-grafted nanotubes nor bare TiO<sub>2</sub> displayed appreciable activity (Table 5, runs 1–2).

The optimal irradiation time of 5 h was ascertained by monitoring photoreduction in the first 7 h of reaction (Figure 6). Results showed that prolonged reaction times (>5 h) led to the decrease of yield in formic acid with the corresponding increment of acetic acid. A plausible explanation could be related to the partial transformation of HCOOH into CH<sub>3</sub>COOH by reaction with methyl radicals (CH<sub>3</sub>), according to the general mechanism proposed by S. Sharifnia et al. [52].

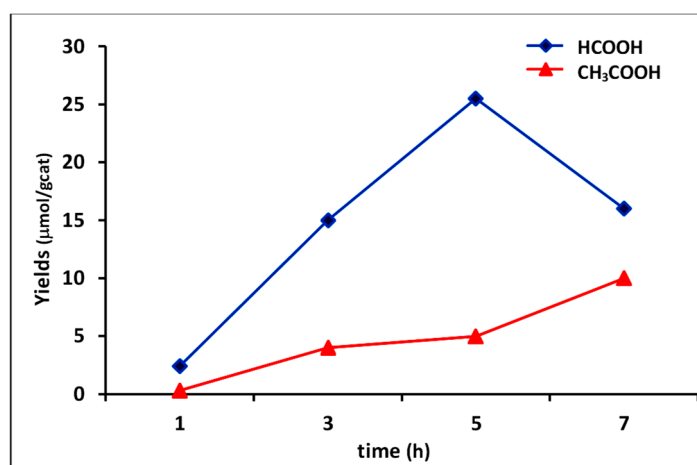


**Scheme 2.** Photoreduction of carbon dioxide.

**Table 5.** Catalytic performance of TiO<sub>2</sub>@PEI-MWCNT hybrids in the photoreduction of CO<sub>2</sub>.

Run	Cat.	% (w/w) of PEI-MWCNTs in Hybrid	Cat. Loading (mg/mL) <sup>a</sup>	Light Source <sup>b</sup>	Photocatalytic Products (μmol·g <sup>-1</sup> Cat.) <sup>c</sup>		
					HCOOH	CH <sub>3</sub> CO <sub>2</sub> H	Total Carbonaceous
1	PEI-MWCNTs (4)	–	7.5	H/S	0.21	0.01	0.22
2	TiO <sub>2</sub>	–	7.5	H/S	1.73	0.01	1.74
3	1A	2.0% <sup>d</sup>	7.5	H/S	2.67	0.38	3.05
4	1C	30.0% <sup>d</sup>	7.5	H/S	5.80	2.73	8.53
5	4A	1.8%	7.5	H/S	4.05	4.30	8.35
6	4B	10.3%	7.5	H/S	13.01	8.49	21.50
7	4C	30.9%	7.5	H/S	29.84	7.46	37.30
8	4C	30.9%	7.5	H	25.50	4.98	30.48
9	4C	30.9%	7.5	S	3.99	23.00	26.99
10	4C <sup>e</sup>	30.9%	7.5	H/S	0.086	0.012	0.096
11	1A	2.0%	25	H/S	0.76	0.15	0.91
12	4A	1.8%	25	H/S	0.51	0.48	0.99
13	4B	10.3%	25	H/S	1.11	2.86	3.97
14	4C	30.9%	25	H/S	16.50	2.44	18.94

<sup>a</sup> Catalyst loading is 150 mg or 500 mg dispersed in 20 mL of water solution. <sup>b</sup> S = SANOLUX HRC UV-VIS lamp 300 W; H = RADIUM Xe-Halogen lamp 400 W. Irradiation time 5 h. <sup>c</sup> Estimated by ionic chromatography. HCOOH and CH<sub>3</sub>COOH formation was neither detected in the dark conditions nor without photocatalyst. <sup>d</sup> Unmodified MWCNTs were hybridized as control composites. <sup>e</sup> Without CO<sub>2</sub>.

**Figure 6.** Monitoring of yields versus time in photocatalysis with composite 4C (experimental conditions of run 7, Table 5).

Composites 1A and 1C bearing unmodified MWCNTs gave formic acid as the major product (Table 5, runs 3–4). In addition, photoreducing power, especially the one leading to formic acid, increased with increasing the percentage of PEI-grafted nanotubes in the composite reaching the maximum level at about 30% (sample 4C, Table 5, runs 5–7).

The head space gas phase was monitored during reaction by means of GC analyses using a specific Barrier Ionization Discharge (BID) detector for revealing the reaction by-products.

Sampling of the gaseous phase above the reaction solution at different time intervals showed a constant composition consisting essentially of O<sub>2</sub> (2%), Argon (5%) and CO<sub>2</sub> (93%). Neither CO, nor H<sub>2</sub> or other gaseous by-products (methane, ethane etc.) were detected during reaction. Notably, the light source proved to have a profound influence on the reaction selectivity: Xe-Halogen lamp (emitting primarily into the visible region) privileged the formation of formic acid, while SANOLUX lamp (with a main radiance in the near UV) favoured the formation of acetic acid (Table 5, runs 8–9).

Catalyst loading affected reaction in a predictable manner. Its increment increased the light scattering, thus limiting photoreducing process. As a consequence, despite the use of a threefold amount of solid catalyst, yields remained almost unchanged (Table 5, runs 11–14).

### 3.4. Catalyst Recycling

Stability and robustness of our nanocatalysts were evaluated by means of recycling experiments (Figure 7). After each run the catalyst powder was recovered by filtration, washed with distilled methanol and water, and then dried under vacuum. Results evidenced a fair to good catalyst stability, with only a little loss of efficiency observed after the first cycle.

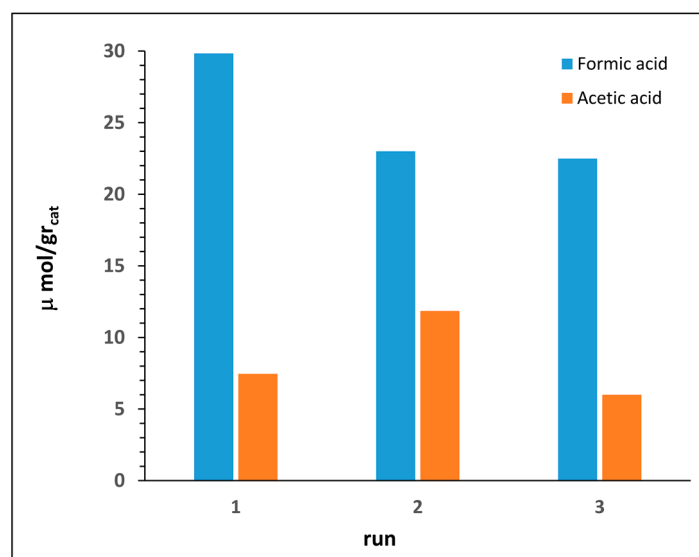


Figure 7. Recycling of photocatalyst nanocomposite 4C.

### 3.5. Mechanistic Insights

The photocatalytic process of CO<sub>2</sub> reduction follows a relative unknown and complex mechanism leading to different products at the same time. Among them, CO, CH<sub>3</sub>OH, HCOOH, CH<sub>4</sub>, HCHO, CH<sub>3</sub>COOH and other light hydrocarbons are mainly observed, with a selectivity affected by a great number of factors [52].

We do not have elements to propose specific mechanisms, but can rationalize in the following points our experimental results attempting also to explain the remarkable enhancement of activity that polyamine modification of TiO<sub>2</sub>/MWCNTs nanocomposites can lead in CO<sub>2</sub> photoreduction:

(i) Firstly, the detection of O<sub>2</sub> into the head space of photoreactor can be considered a clear evidence that water is the sacrificial reductant for CO<sub>2</sub>.

(ii) Secondly, the high chemisorption capacity of TiO<sub>2</sub>@PEI-MWCNTs (4C) (18 mL<sub>CO<sub>2</sub></sub>/g) is most probably the key reason for its enhanced photoreducing ability, due to kinetic effects. Indeed, reaction of CO<sub>2</sub> with NH<sub>2</sub> groups forms carbamate, thus leading to the activation of carbon dioxide, because carbamate is believed to have a higher reactivity than the linear CO<sub>2</sub> molecule (Figure 8) [24]. This assumption is corroborated by FT-IR analyses (Figure 9) of (4C) under photocatalytic conditions before and after CO<sub>2</sub> bubbling, in which the peak at 1489 cm<sup>-1</sup> appeared that can be attributed to the carbamate COO<sup>-</sup> stretching [53,54].

(iii) Thirdly, an electronic effect of PEI could also be invoked in the UV range. It has been extensively approved that MWCNTs can narrow the band gap of TiO<sub>2</sub> extending light absorption to longer wavelength region. The red shift observed in Figure 5 confirms such a hypothesis. In addition, due to their graphite-like structure, MWCNTs are considered as a channel for electron storage, functioning as electron acceptors from higher conduction band of TiO<sub>2</sub>, thus inhibiting the recombination rate of electron-hole pairs through the transfer of electrons [24]. This is extremely crucial as the slower recombination rate leaves more holes in TiO<sub>2</sub>, promoting higher oxidation rate of water and thus enhancing reduction of CO<sub>2</sub> (Figure 10).

In this context, it can be assumed that PEI-grafting, from one hand, does not modify the graphite-like structure of CNTs thus allowing them to continue their action of narrowing the band gap of titania, while, from the other hand, can enhance the photocatalytic activity of  $\text{TiO}_2$  into the UV range due to the auxochrome effect.

Notably, lowering of crystallinity experienced by  $\text{TiO}_2$  as a consequence of hybridization (Figure 4c) does not influence catalytic performance, as this detrimental effect is counterbalanced by the enhancement of both the electron scavenging and  $\text{CO}_2$  capture capacity of nanocomposite by virtue of PEI-CNTs conjugation.

(iv) Searching for further confirmations on the effect on photocatalytic activity of PEI-conjugation with  $\text{TiO}_2/\text{MWCNTs}$  composites, we investigated the photoreduction of the organic dye UBA, (Scheme 3) a model substrate commonly used to investigate electron transfer reactions [18,44,45]. Irradiation was performed with UV light using a mercury lamp ( $\lambda > 250 \text{ nm}$ ) and photoreduction was checked monitoring the colour change from blue (the colour of UBA anthraquinonic structure) to yellow (due to UBA reduced form).

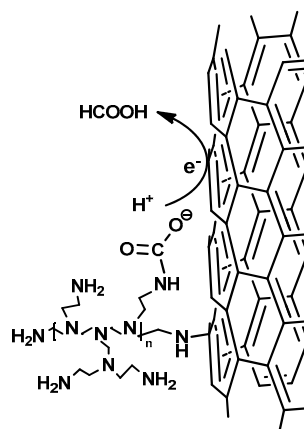


Figure 8. Activation of  $\text{CO}_2$  in photoreduction by PEI through carbamate formation.

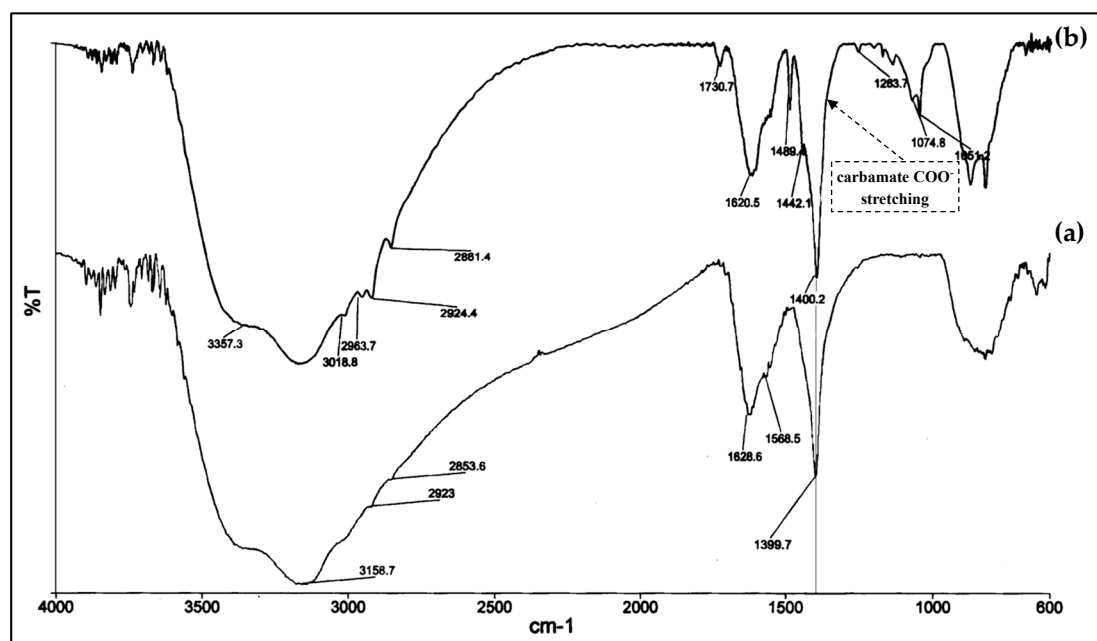
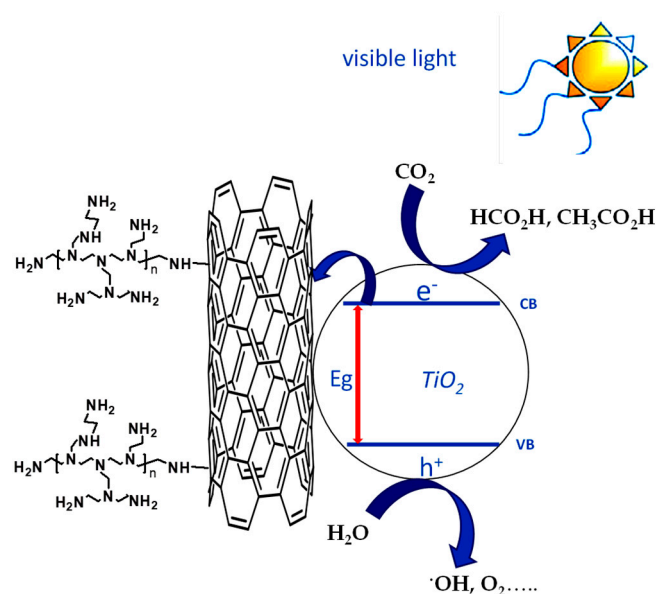
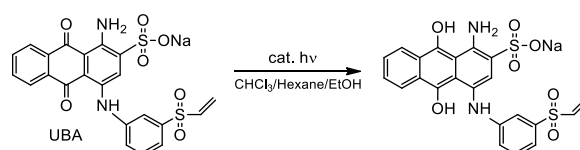


Figure 9. FT-IR images of  $\text{TiO}_2@\text{PEI-MWCNTs}$  (4C) under photocatalytic conditions (a) before and (b) after  $\text{CO}_2$  bubbling.



**Figure 10.** Effect of PEI conjugation on separation of photogenerated electron-hole pairs for TiO<sub>2</sub>@PEI-MWCNTs nanocomposite.



**Scheme 3.** photoreduction of UBA.

Differences in absorbance ( $\Delta$ Abs) acquired at 587 nm as a function of irradiation time were reported (Figure 11) [44,45]. Results clearly evidenced a higher reducing capability of the TiO<sub>2</sub>@PEI-MWCNTs (**4C**) compared to the bare TiO<sub>2</sub>. Indeed, with **4C** as catalyst, an almost complete photoreduction of UBA was observed in the first 30 min of reaction, with the  $\Delta$ Abs value of 0.98. After that, the  $\Delta$ Abs value reached a plateau.

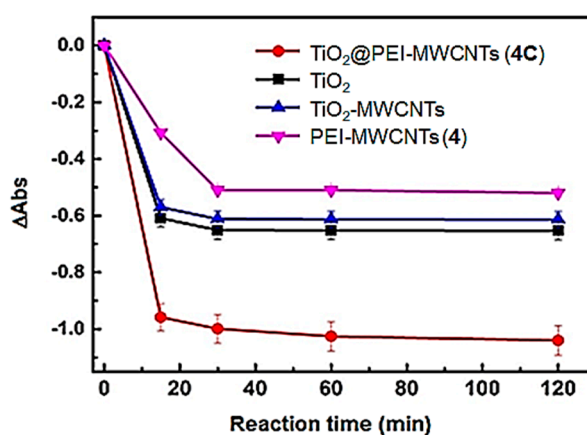


**Figure 11.** Time course of UBA bleaching monitored at 587 nm. Data are reported as mean value of three replicates  $\pm$  standard deviation.

Conversely, with bare TiO<sub>2</sub>, the  $\Delta$ Abs was detected to be 0.6 indicating that titania alone can promote UBA photoreduction up to the 60% in the first 30 min of irradiation. Next, despite prolonged irradiation the  $\Delta$ Abs remained constant.

Two further control experiments were performed using PEI-MWCNTs (4) and TiO<sub>2</sub>@MWCNTs (1C) sample as catalysts, respectively. The former resulted in a 30% photoreduction of UBA during the first 30 min of irradiation, while the latter gave rise to 56% of UBA photoreduction, displaying a reduction capacity comparable with that of bare TiO<sub>2</sub> and lower than that observed for TiO<sub>2</sub>@PEI-MWCNTs (4C). This beneficial role played by the functionalization with PEI could be explained with the auxochrome effect in the UV region exerted by amino and hydroxyl groups of PEI-modified composites (clearly visible in the UV spectrum of Figure 5), and is in accordance with the accepted principles “the higher the light absorption, the more the photoexcited electron–hole pairs” or also “the higher the reflectance the higher the activity” [55].

In addition, the disappointing results of UBA reduction assisted by PEI-MWCNTs (4), pointed out that an efficient UBA photoreduction is promoted only in the presence of TiO<sub>2</sub>, especially upon its interaction with MWCNTs efficiently mediated by PEI. Remarkably, the sample TiO<sub>2</sub>-MWCNTs (1C) showed a lower photocatalytic efficiency respect to the TiO<sub>2</sub>@PEI-MWCNTs (4C), despite they have a comparable specific surface area (Table 3: 299.2 m<sup>2</sup>/g and 304.2 m<sup>2</sup>/g, respectively). Such a behaviour further highlights the beneficial role played by the functionalization of MWCNTs with the PEI in the achievement of a highly photoactive nanocomposite.

(v) Finally, a special attention deserves the photoreduction selectivity towards the two main photoreduction products HCOOH/CH<sub>3</sub>COOH. Results in Table 5 clearly show that formation of HCOOH increases with increasing of PEI-grafted MWCNTs percentage in the nanocomposite, with the best yields reached with 30% ca. of carbon dopants (catalyst 4C, Table 5, runs 7–8, 14). This trend is in line with the above mentioned assumptions.

More difficult is the rationale for the formation of CH<sub>3</sub>COOH. This product is more rarely observed, even if is the major product in water suspension [56], like in our case, or using TiO<sub>2</sub> doped with metals like Cu, Rh and Ru [56–58]. From results in Table 5 emerged that acetic acid formation depends on the nature of light source, with highest value reached using SANOLUX UV lamp (Table 5, run 9). This result indicates that formation of acetic acid is favoured by the UV-component of radiation and seems to be in accordance with the auxochrome effect of PEI into the UV region (Figure 5).

We do not have other elements explaining this phenomenon, and further efforts are needed to unravel the complex mechanistic aspects underlying the photocatalytic activity of these new materials.

#### 4. Conclusions

In summary, we have found that polyethylenimine (PEI) anchored onto multiwalled carbon nanotubes can strongly enhance photocatalytic performances of TiO<sub>2</sub>/MWCNTs composites, rendering these materials efficient photocatalysts for CO<sub>2</sub> conversion into formic and acetic acids. The simultaneous presence of PEI and CNTs is essential for catalysis, as demonstrated by the high sorbent capacity of TiO<sub>2</sub>@PEI-MWCNTs (4C) (18 mL/g) that enables both CO<sub>2</sub> capture and activation, most probably via carbamate formation. Bleaching experiments corroborate in part the beneficial role of PEI in enhancing the photoreducing power of TiO<sub>2</sub>/MWCNTs composites in the UV range by means of a plausible auxochrome effect.

To the best of our knowledge, this is the first example in the literature in which amines-grafted CNTs materials can function as TiO<sub>2</sub> co-catalysts for converting CO<sub>2</sub> into carboxylic acids. We hope this work opens new avenues for carbon recycling using renewable sources.

**Supplementary Materials:** The following are available online at <http://www.mdpi.com/1996-1944/11/2/307/s1>. Detailed XRD, XPS, SEM analyses, CO<sub>2</sub> photoreduction apparatus, Spectra of emission lamps (Figures S1–S6). **Figure S1:** Schematic representation of apparatus for measuring CO<sub>2</sub> adsorption/desorption ability, **Figure S2:** XRD patterns of samples 4, 1A, 4A-B, **Figure S3: High-resolution N1s signal**, **Figure S4:** SEM image of (A) sample TiO<sub>2</sub>@MWCNTs 1A. SEM images of sample TiO<sub>2</sub>@PEI-MWCNTs 4C at (B) 2 μm, (C) 200 nm and (D) 100 nm of magnification level, **Figure S5:** Schematic of CO<sub>2</sub> photoreduction apparatus, Figure S6: Emission spectra of (a) HRC UV-VIS lamp 300 W (Sanolux) and (b) Xe-Halogen lamp 400 W (Radium).

**Acknowledgments:** This research was supported by: Regione Puglia MIUR PON Ricerca e Competitività 20072013 Avviso 254/Ric. del 18/05/2011, Project PONA3 00369 “Laboratorio SISTEMA”, the Regione Puglia Project 3Z3VZ46 “RESTAUREO”, Apulia Region funded NanoApulia (MDI6SR) and Project RELA-VALBIOR, Network of Laboratories for Scientific Research (Italy). Project PON03PE\_00004\_1, “MAIND” MATERIALI eco-innovativi e tecnologie avanzate per l’INDustria Manifatturiera e delle costruzioni. The authors wish to thank Ms Annarita Armenise for skilful assistance.

**Author Contributions:** M.C. performed the experiments of photoreduction of CO<sub>2</sub>; F.P. performed the experiments of UBA, R.C. and V.M. performed the analysis of SEM; TEM, BET; F.F. performed the XPS and TGA analysis, A.F. and A.M. performed the XRD analysis, R.C. and L.C. analyzed the data; C.F., L.D. and A.N. conceived and designed the experiments and wrote the paper.

**Conflicts of Interest:** The authors declare no conflict of interest.

## References

1. Kim, D.; Sakimoto, K.K.; Hong, D.; Yang, P. Artificial Photosynthesis for Sustainable Fuel and Chemical Production. *Angew. Chem. Int. Ed.* **2015**, *54*, 2–10. [[CrossRef](#)] [[PubMed](#)]
2. Álvarez, A.; Bansode, A.; Urakawa, A.; Bavykina, A.V.; Wezendonk, T.A.; Makkee, M.; Gascon, J.; Kapteijn, F. Challenges in the Greener Production of Formates/Formic Acid, Methanol, and DME by Heterogeneously Catalyzed CO<sub>2</sub> Hydrogenation Processes. *Chem. Rev.* **2017**, *117*, 9804–9838. [[CrossRef](#)] [[PubMed](#)]
3. Inoue, T.; Fujishima, A.; Konishi, S.; Honda, K. Photoelectrocatalytic reduction of carbon dioxide in aqueous suspensions of semiconductor powders. *Nature* **1979**, *277*, 637–638. [[CrossRef](#)]
4. Li, K.; Peng, B.; Peng, T. Recent Advances in Heterogeneous Photocatalytic CO<sub>2</sub> Conversion to Solar Fuels. *ACS Catal.* **2016**, *6*, 7485–7527. [[CrossRef](#)]
5. Guan, G.; Kida, T.; Yoshida, A. Reduction of carbon dioxide with water under concentrated sunlight using photocatalyst combined with Fe-based catalyst. *Appl. Catal. B* **2003**, *41*, 387–396. [[CrossRef](#)]
6. Wang, W.N.; An, W.J.; Ramalingam, B.; Mukherjee, S.; Niedzwiedzki, D.M.; Gangopadhyay, S.; Biswas, P. Size and structure matter: enhanced CO<sub>2</sub> photoreduction efficiency by size-resolved ultrafine Pt nanoparticles on TiO<sub>2</sub> single crystals. *J. Am. Chem. Soc.* **2012**, *134*, 11276–11281. [[CrossRef](#)] [[PubMed](#)]
7. Gui, M.M.; Chai, S.P.; Mohamed, A.R. Modification of MWCNT@ TiO<sub>2</sub> core-shell nanocomposites with transition metal oxide dopants for photoreduction of carbon dioxide into methane. *Appl. Surf. Sci.* **2014**, *319*, 37–43. [[CrossRef](#)]
8. Gui, M.M.; Wonga, W.M.P.; Chai, S.P.; Mohamed, A.R. One-pot synthesis of Ag-MWCNT@ TiO<sub>2</sub> core-shell nanocomposites for photocatalytic reduction of CO<sub>2</sub> with water under visible light irradiation. *Chem. Eng. J.* **2015**, *278*, 272–278. [[CrossRef](#)]
9. Mele, G.; Annese, C.; D’Accolti, L.; De Riccardis, A.; Fusco, C.; Palmisano, L.; Scarlino, A.; Vasapollo, G. Photoreduction of Carbon Dioxide to Formic Acid in Aqueous Suspension: A Comparison between Phthalocyanine/TiO<sub>2</sub> and Porphyrin/TiO<sub>2</sub> Catalysed Processes. *Molecules* **2015**, *20*, 396–415. [[CrossRef](#)] [[PubMed](#)]
10. Ong, W.-J.; Gui, M.M.; Chai, S.-P.; Mohamed, A.R. Direct growth of carbon nanotubes on Ni/ TiO<sub>2</sub> as next generation catalysts for photoreduction of CO<sub>2</sub> to methane by water under visible light irradiation. *RSC Adv.* **2013**, *3*, 4505–4509. [[CrossRef](#)]
11. Xu, H.; Ouyang, S.; Liu, L.; Wang, D.; Kako, T.; Ye, J. Porous-structured Cu<sub>2</sub>O/TiO<sub>2</sub> nanojunction material toward efficient CO<sub>2</sub> photoreduction. *Nanotechnology* **2014**, *25*, 165402–165410. [[CrossRef](#)] [[PubMed](#)]
12. Suna, Z.; Wanga, H.; Wua, Z.; Wang, L. g-C<sub>3</sub>N<sub>4</sub> based composite photocatalysts for photocatalytic CO<sub>2</sub> reduction. *Catal. Today* **2018**, *300*, 160–172. [[CrossRef](#)]
13. Liu, Y.; Zhou, S.; Li, J.; Wang, Y.; Jiang, G.; Zhao, Z.; Liu, B.; Gong, X.; Duan, A.; Liu, Y.; et al. Photocatalytic reduction of CO<sub>2</sub> with water vapor on surface La-modified TiO<sub>2</sub> nanoparticles with enhanced CH<sub>4</sub> selectivity. *Appl. Catal. B.* **2015**, *168–169*, 125–131. [[CrossRef](#)]

14. Xia, X.-H.; Jia, Z.-J.; Yu, Y.; Liang, Y.; Wang, Z.; Ma, L.-L. Preparation of multi-walled carbon nanotube supported TiO<sub>2</sub> and its photocatalytic activity in the reduction of CO<sub>2</sub> with H<sub>2</sub>O. *Carbon* **2007**, *45*, 717–721. [[CrossRef](#)]
15. Tian, L.; Ye, L.; Deng, K.; Zan, L. TiO<sub>2</sub>/carbon nanotube hybrid nanostructures: Solvothermal synthesis and their visible light photocatalytic activity. *J. Solid State Chem.* **2011**, *184*, 1465–1471. [[CrossRef](#)]
16. Gao, B.; Chen, G.Z.; Puma, G.L. Carbon nanotubes/titanium dioxide (CNTs/TiO<sub>2</sub>) nanocomposites prepared by conventional and novel surfactant wrapping sol-gel methods exhibiting enhanced photocatalytic activity. *Appl. Catal. B.* **2009**, *89*, 503–509. [[CrossRef](#)]
17. Cong, Y.; Li, X.; Qin, Y.; Dong, Z.; Yuan, G.; Cui, Z.; Lai, X. Carbon-doped TiO<sub>2</sub> coating on multiwalled carbon nanotubes with higher visible light photocatalytic activity. *Appl. Catal. B.* **2011**, *107*, 128–134. [[CrossRef](#)]
18. Kongkanand, A.; Kamat, P.V. Electron Storage in Single Wall Carbon Nanotubes. Fermi Level Equilibration in Semiconductor-SWCNT Suspensions. *ACS Nano* **2007**, *1*, 13–21. [[CrossRef](#)] [[PubMed](#)]
19. Zhang, Y.; Tang, Z.-R.; Fu, X.; Xu, Y.-J. TiO<sub>2</sub>-Graphene Nanocomposites for Gas-Phase Photocatalytic Degradation of Volatile Aromatic Pollutant: Is TiO<sub>2</sub>-Graphene Truly Different from Other TiO<sub>2</sub>-Carbon Composite Materials? *ACS Nano* **2010**, *4*, 7303–7314. [[CrossRef](#)] [[PubMed](#)]
20. Xie, S.; Zhang, Q.; Liu, G.; Wang, Y. Photocatalytic and photoelectrocatalytic reduction of CO<sub>2</sub> using heterogeneous catalysts with controlled nanostructures. *Chem. Commun.* **2016**, *52*, 35–59. [[CrossRef](#)] [[PubMed](#)]
21. Meng, X.; Ouyang, S.; Kako, T.; Li, P.; Liu, Q.; Wang, T.; Ye, J. Photocatalytic CO<sub>2</sub> conversion over alkali modified TiO<sub>2</sub> without loading noble metal cocatalyst. *Chem. Commun.* **2014**, *50*, 11517–11519. [[CrossRef](#)] [[PubMed](#)]
22. Xie, S.J.; Wang, Y.; Zhang, Q.H.; Fan, W.Q.; Deng, W.P.; Wang, Y. Photocatalytic reduction of CO<sub>2</sub> with H<sub>2</sub>O: significant enhancement of the activity of Pt-TiO<sub>2</sub> in CH<sub>4</sub> formation by addition of MgO. *Chem. Commun.* **2013**, *49*, 2451–2453. [[CrossRef](#)] [[PubMed](#)]
23. Fu, Y.; Sun, D.; Chen, Y.; Huang, R.; Ding, Z.; Fu, X.; Li, Z. An Amine-Functionalized Titanium Metal-Organic Framework Photocatalyst with Visible-Light-Induced Activity for CO<sub>2</sub> Reduction. *Angew. Chem. Int. Ed.* **2012**, *51*, 3364–3367. [[CrossRef](#)] [[PubMed](#)]
24. Liao, Y.; Cao, S.W.; Yuan, Y.; Gu, Q.; Zhang, Z.; Xue, C. Efficient CO<sub>2</sub> Capture and Photoreduction by Amine-Functionalized TiO<sub>2</sub>. *Chem. Eur. J.* **2014**, *20*, 10220–10222. [[CrossRef](#)] [[PubMed](#)]
25. Liu, G.; Xie, S.; Zhang, Q.; Tian, Z.; Wang, Y. Carbon dioxide-enhanced photosynthesis of methane and hydrogen from carbon dioxide and water over Pt-promoted polyaniline-TiO<sub>2</sub> nanocomposites. *Chem. Commun.* **2015**, *51*, 13654–13657. [[CrossRef](#)] [[PubMed](#)]
26. Hsu, S.-C.; Lu, C.; Su, F.; Zeng, W.; Chen, W. Thermodynamics and regeneration studies of CO<sub>2</sub> adsorption on multiwalled carbon nanotubes. *Chem. Eng. Sci.* **2010**, *65*, 1354–1361. [[CrossRef](#)]
27. Mansoor, A.; Hoseini, V. Development of MWCNT@MIL-101 hybrid composite with enhanced adsorption capacity for carbon dioxide. *Chem. Eng. J.* **2012**, *191*, 326–330. [[CrossRef](#)]
28. Lee, M.-S.; Park, S.-J. Silica-coated multi-walled carbon nanotubes impregnated with polyethyleneimine for carbon dioxide capture under the flue gas condition. *J. Solid State Chem.* **2015**, *226*, 17–23. [[CrossRef](#)]
29. Dillon, E.P.; Crouse, C.A.; Barron, A.R. Synthesis, Characterization, and Carbon Dioxide Adsorption of Covalently Attached Polyethyleneimine-Functionalized Single-Wall Carbon Nanotubes. *ACS Nano* **2007**, *2*, 156–164. [[CrossRef](#)] [[PubMed](#)]
30. Liu, Q.; Shi, J.; Wang, Q.; Tao, M.; He, Y.; Shi, Y. Carbon Dioxide Capture with Polyethylenimine-Functionalized Industrial-Grade Multiwalled Carbon Nanotubes. *Ind. Eng. Chem. Res.* **2014**, *53*, 17468–17475. [[CrossRef](#)]
31. Yang, B.; Hu, H.; Yu, Q.; Zhang, X.; Lia, Z.; Lei, L. Pretreated multiwalled carbon nanotube adsorbents with amine-grafting for removal of carbon dioxide in confined spaces. *RSC Adv.* **2014**, *4*, 56224–56234. [[CrossRef](#)]
32. Khalili, S.; Ghoreyshi, A.A.; Jahanshahi, M.; Pirzadeh, K. Enhancement of Carbon Dioxide Capture by Amine-Functionalized Multi-Walled Carbon Nanotube. *Clean Soil Air Water* **2013**, *41*, 939–948. [[CrossRef](#)]
33. Casiello, M.; Iannone, F.; Cotugno, P.; Monopoli, M.; Cioffi, N.; Ciminale, F.; Trzeciak, A.M.; Nacci, A. Copper(II)-catalysed oxidative carbonylation of aminols and amines in water: A direct access to oxazolidinones, ureas and carbamates. *J. Mol. Cat. A. Chem.* **2015**, *407*, 8–14. [[CrossRef](#)]
34. Iannone, F.; Casiello, M.; Monopoli, A.; Cotugno, P.; Sportelli, M.C.; Picca, R.A.; Cioffi, N.; Dell’Anna, M.M.; Nacci, A. Ionic liquids/ZnO nanoparticles as recyclable catalyst for polycarbonate depolymerization. *J. Mol. Cat. A Chem.* **2017**, *426*, 107–116. [[CrossRef](#)]

35. Annese, C.; Abbrescia, D.I.; Catucci, L.; D'Accolti, L.; Denora, N.; Fanizza, I.; Fusco, C.; La Piana, G. Site-dependent biological activity of valinomycin analogs bearing derivatizable hydroxyl sites. *J. Pep. Sci.* **2013**, *19*, 751–757. [[CrossRef](#)] [[PubMed](#)]
36. Lopalco, A.; Stella, V.J. Effect of molecular structure on the relative hydrogen peroxide scavenging ability of some  $\alpha$ -keto carboxylic acids. *J. Pharm. Sci.* **2016**, *105*, 2879–2885. [[CrossRef](#)] [[PubMed](#)]
37. Dentuto, P.L.; Catucci, L.; Cosma, P.; Fini, P.; Agostiano, A.; D'Accolti, L.; Trevithick-Sutton, C.C.; Foote, C.S. Effect of cyclodextrins on the physicochemical properties of chlorophyll a in aqueous solution. *J. Phys. Chem. B* **2005**, *109*, 1313–1317. [[CrossRef](#)] [[PubMed](#)]
38. Annese, C.; D'Accolti, L.; Filardi, R.; Tommasi, I.; Fusco, C. Oxidative cleavage of lactams in water using dioxiranes: an expedient and environmentally-safe route to  $\omega$ -nitro acids. *Tet. Lett.* **2013**, *54*, 515–517. [[CrossRef](#)]
39. D'Accolti, L.; Annese, C.; De Riccardis, A.; De Giglio, E.; Cafagna, D.; Fanelli, F.; Fusco, C. Dioxirane-Mediated Heterogeneous Epoxidations with Potassium Caroate: A Solid Catalyst Bearing Anchored Ketone Moieties. *Eur. J. Org. Chem.* **2012**, *24*, 4616–4621. [[CrossRef](#)]
40. Annese, C.; D'Accolti, L.; Fusco, C.; Curci, R. Selective Hydroxylation of Methane by Dioxiranes under Mild Conditions. *Org. Lett.* **2011**, *13*, 2142–2144. [[CrossRef](#)] [[PubMed](#)]
41. Annese, C.; D'Accolti, L.; Armuzza, V.; Da Ros, T.; Fusco, C. Epoxidation of multi-walled carbon nanotubes by organocatalytic oxidation. *Eur. J. Org. Chem.* **2015**, 3063–3068. [[CrossRef](#)]
42. Annese, C.; D'Accolti, L.; Giambastiani, G.; Mangone, A.; Milella, A.; Tuci, G.; Fusco, C. Tunable epoxidation of single-walled carbon nanotubes by isolated methyl(trifluoromethyl)dioxirane. *Eur. J. Org. Chem.* **2014**, *8*, 1666–1671. [[CrossRef](#)]
43. Mele, G.; Annese, C.; De Riccardis, A.; Fusco, C.; Palmisano, L.; Vasapollo, G.; D'Accolti, L. Turning lipophilic phthalocyanines/TiO<sub>2</sub> composites into efficient photocatalysts for the conversion of CO<sub>2</sub> into formic acid under UV-Vis light irradiation. *Appl. Catal. A* **2014**, *481*, 169–172. [[CrossRef](#)]
44. Cozzoli, P.D.; Fanizza, E.; Comparelli, R.; Curri, M.L.; Agostiano, A.; Laub, D.L. Role of Metal Nanoparticles in TiO<sub>2</sub>/Ag Nanocomposite-Based Microheterogeneous Photocatalysis. *J. Phys. Chem. B* **2004**, *108*, 9623–9630. [[CrossRef](#)]
45. George, C.; Dorfs, D.; Bertoni, G.; Falqui, A.; Genovese, A.; Pellegrino, T.; Roig, A.; Quarta, A.; Comparelli, R.; Curri, M.L.; Cingolani, R.; Manna, L. A Cast-Mold Approach to Iron Oxide and Pt/Iron Oxide Nanocontainers and Nanoparticles with a Reactive Concave Surface. *J. Am. Chem. Soc.* **2011**, *133*, 2205–2217. [[CrossRef](#)] [[PubMed](#)]
46. Aviles, F.; Cauich-Rodriguez, J.V.; Moo-Tah, L.A.; May-Pat, A.; Vargas-Coronado, R. Evaluation of mild acid oxidation treatments for MWCNT functionalization. *Carbon* **2009**, *47*, 2970–2975. [[CrossRef](#)]
47. Shen, X.; Du, H.; Mullins, R.H.; Kommalapati, R.R. Polyethylenimine Applications in Carbon Dioxide Capture and Separation: From Theoretical Study to Experimental Work. *Energy Technol.* **2017**, *5*, 822–833. [[CrossRef](#)]
48. Miranda, S.M.; Romanosc, G.E.; Likodimos, V.; Marquesa, R.R.N.; Favvasc, E.P.; Katsarosc, F.K.; Stefanopoulosc, K.L.; Vilarb, V.J.P.; Faria, J.L.; Falarasc, P.; et al. Pore structure, interface properties and photocatalytic efficiency of hydration/dehydration derived TiO<sub>2</sub>/CNT composites. *Appl. Catal. B Environ.* **2014**, *147*, 65–81. [[CrossRef](#)]
49. Natarajan, T.S.; Lee, J.Y.; Bajaj, H.C.; Jo, W.-K.; Tayade, R.J. Synthesis of multiwall carbon nanotubes/TiO<sub>2</sub> nanotube composites with enhanced photocatalytic decomposition efficiency. *Catal. Today* **2017**, *282*, 13–23. [[CrossRef](#)]
50. Gui, M.M.; Chai, S.-P.; Xub, B.-Q.; Mohamed, A.R. Visible-light-driven MWCNT@TiO<sub>2</sub> core-shell nanocomposites and the roles of MWCNTs on the surface chemistry, optical properties and reactivity in CO<sub>2</sub> photoreduction. *RSC Adv.* **2014**, *4*, 24007–24013. [[CrossRef](#)]
51. Chen, Y.; Bian, J.; Qi, L.; Liu, E.; Fan, J. Efficient Degradation of Methylene Blue over Two-Dimensional Au/TiO<sub>2</sub> Nanosheet Films with Overlapped Light Harvesting Nanostructures. *J. Nanomater.* **2015**, *16*, 254. [[CrossRef](#)]
52. Karamian, E.; Sharifnia, S. On the general mechanism of photocatalytic reduction of CO<sub>2</sub>. *J. CO<sub>2</sub> Util.* **2016**, *16*, 194–203. [[CrossRef](#)]

53. Tumuluri, U.; Isenberg, M.; Tan, C.-S.; Chuang, S.S.C. In situ infrared study of the effect of amine density on the nature of adsorbed CO<sub>2</sub> on amine-functionalized solid sorbents. *Langmuir* **2014**, *30*, 7405–7413. [[CrossRef](#)] [[PubMed](#)]
54. Wilfong, W.C.; Srikanth, C.S.; Chuang, S.S.C. In situ ATR and DRIFTS studies of the nature of adsorbed CO<sub>2</sub> on tetraethylenepentamine films. *ACS Appl. Mater. Interfaces* **2014**, *6*, 13617–13626. [[CrossRef](#)] [[PubMed](#)]
55. Xu, Y.-H.; Wang, L.-Y.; Zhang, Q.; Zheng, S.-J.; Li, X.-J.; Huang, C. Correlation between photoreactivity and photophysics of sulfated TiO<sub>2</sub> photocatalyst. *Mater. Chem. Phys.* **2005**, *92*, 470–474. [[CrossRef](#)]
56. Nazimek, B.; Czech, B. Artificial photosynthesis-CO<sub>2</sub> towards methanol. *IOP Conf. Ser. Mater. Sci. Eng.* **2011**, *19*, 012010. [[CrossRef](#)]
57. Srinivas, B.; Shubhamangala, B.; Lalitha, K.; Reddy, P.A.K.; Kumari, V.D.; Subrahmanyam, M.; De, B.R. Photocatalytic Reduction of CO<sub>2</sub> over Cu-TiO<sub>2</sub>/Molecular Sieve 5A Composite. *Photochem. Photobiol.* **2011**, *87*, 995–1001. [[CrossRef](#)] [[PubMed](#)]
58. Ishitani, O.; Inoue, C.; Suzuki, Y.; Ibusuki, T.J. Photocatalytic reduction of carbon dioxide to methane and acetic acid by an aqueous suspension of metal-deposited TiO<sub>2</sub>. *Photochem. Photobiol. A Chem.* **1993**, *72*, 269–271. [[CrossRef](#)]



© 2018 by the authors. Licensee MDPI, Basel, Switzerland. This article is an open access article distributed under the terms and conditions of the Creative Commons Attribution (CC BY) license (<http://creativecommons.org/licenses/by/4.0/>).